Port-Hamiltonian model and load balancing for DC-microgrid lift systems

Thanh Hung Pham, Ionela Prodan, Denis Genon-Catalot, Laurent Lefèvre

Port-Hamiltonian model and load balancing for DC-microgrid lift systems

T. Hung Pham, I. Prodan, D. Genon-Catalot and L. Lefèvre*

Univ. Grenoble Alpes, LCIS, F-26902, France
* *corresponding author (Laurent.Lefevre@lcis.grenoble-inp.fr)*

Abstract: This paper considers the problem of modeling a multi-source lift system where power balancing - realized through a power DC bus - should be optimally controlled. The system includes the mechanical part, a Salient Permanent Magnet Synchronous Machine (SPMSM), a battery energy storage unit, a super-capacitor, a solar panel (PV) generation unit as well as the corresponding converters to DC-links. This microgrid is connected to a three-phase utility (external) grid. A port-Hamiltonian model is proposed for the system. It includes the descriptions of nonlinear characteristics and the limitations for each components as well as some typical operation demands. Then, different optimization objectives are formulated in view of an efficient energy management within the microgrid system.

Keywords: DC microgrid, autonomous lifts, port-Hamiltonian systems, load balancing

1. INTRODUCTION

An important aspect of nowadays energy systems is that the collaborative communication between the many subsystems extends substantially the dimension of the controlled system (see, for instance, Nuno et al. (2013) or Schiffer et al. (2014)). This issue can be tackled by dividing the global system into a network of many autonomous subsystems that can operate independently as well as cooperatively. These subsystems are usually called microgrids which are autonomous from both control and energy aspects.

Microgrid systems and energy management in general, represent an actual area of research. Therefore, many works are providing different modeling and control approaches depending on the global objectives of the corresponding systems. Some works propose a predictive control framework which takes into consideration the cost values, power consumption and generation profiles, as well as specific constraints (see Prodan and Zio (2014); Parisio et al. (2014)). However, only simplified linear models for the microgrid components are employed. This is also the case for recent works on distributed or decentralized control of microgrids (see, for instance, Yang et al. (2014); Lagorse et al. (2010)). Other works consider more realistic (and complex) models for the microgrid or some of its components. For instance, source and supercapacitor models may be found in Mohammedi et al. (2013). They are useful to compute explicitly the power balance equation and for the design of some Passivity-Based Control (PBC). However this work consider only a global model and do not decompose it into an interconnection structure and connected components. They are therefore not appropriate for developing a decentralized approach to solve the power balancing problem for networks of non linear components.

In the present paper we introduce the port-Hamiltonian (PH) formulation to express explicitly the power interconnection structure between components of the microgrid and take into account the nonlinear dynamics in the energy dissipations, storages and conversions in these components. This unified model of all the subsystems interconnected through the microgrid interconnection structure represents the lift system as unique hierarchical energy network which will be useful for the efficient energy management (optimal power balancing). Furthermore, each subsystem will be presented in the paper with its constraints and local objectives. On the global view, constraints and objectives of the whole system are analyzed as well.

The investigated lift system microgrid is represented in Fig. 1. It consists in the parallel connection of energy generation systems, storage devices and controlled loads to the high voltage DC-link which is modeled as a capacitor. Generally, the storage and the load can exchange energy between them. This exchange can be implemented by the bi-direction converters that connect the subsystems to the DC-link. Specifically, the load in this case is the elevator system that transforms the electrical energy to/from mechanical potential energy.

The paper is organized as follows. Section 2 details the models of all the components and the converters connected to the DC bus. In the section 3, the constraints of each component are formulated. Then, in section 4, the local/global objectives of the system are presented with some proposed cost functions. Finally in section 5 we draw the conclusion and present the future work. In the appendix, the reader will find tables with notations for all the parameters and variables used throughout the paper. The parameters values for the SPMSM have been identified on the real system with methods described in Pham et al. (2014).

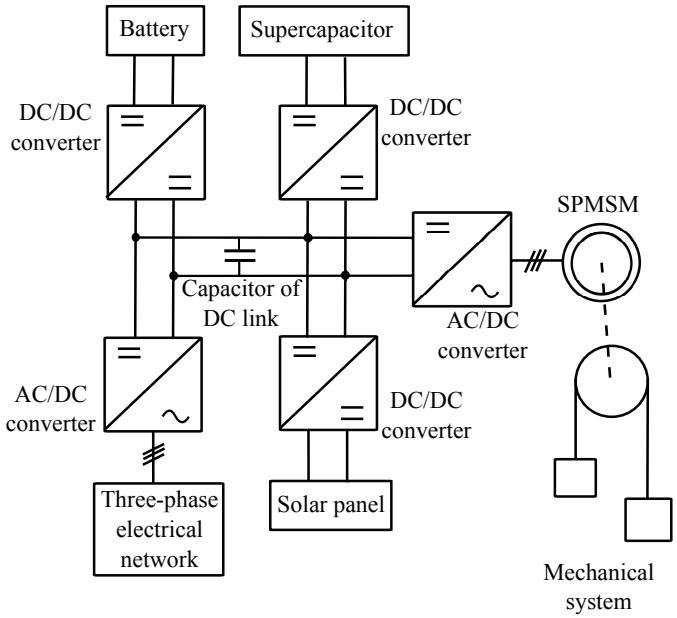

Fig. 1. Lift system microgrid architecture

2. SYSTEM AND MODEL DESCRIPTION

2.1 DC microgrid

The microgrid system considered in this research (see Fig. 1) is made of the connection of three types of physical components: loads, internal energy storages and external energy sources. Usually components are consuming or producing different types of energy: mechanical, electrical, chemical, solar energy, etc. For regulating the energy flow between them, components are connected to DC-links through the corresponding converters (see Paire et al. (2010)).

The energy storage devices are required in order to guarantee the smooth operation in the case of interruption of the external grid. Furthermore, it helps reducing the electrical cost by storing energy in (electricity) low price period (or when renewable energy unit is available) and reusing it in high price period (or when renewable energy unit is unavailable). The most popular storage device is the battery which stores the received energy in the chemical form. Likewise, the supplementary supercapacitor is added for providing the high instantaneous power demand during the start up phases of the SPMSM. Each of them is connected to the DC-link through a DC/DC converter.

The load investigated in our works contains a mechanical system, a SPMSM and its respective DC/AC converter. In that the main parts of the mechanical system are the cabin and the counterweight. Counterweight is added to reduce the necessary torque of the motor needed to pull the cabin. This mechanical system is connected directly with the motor without gearbox to avoid any unnecessary energy dissipation. From an energetic point of view, there are thus two typical operation modes: energy consumption when the magnet torque of the motor has the same direction with rotors speed, and energy production in the opposite case.

For the explicit representation of all the power exchanges throughout the system, we will make use of the Bond Graph notations to represent the microgrid structure as depicted in Fig. 2. As it can be observed, all components are connected in parallel (depicted by "0" element at the graph center) to the DC bus, including the DC-link capacitor itself. The considered sources are the external grid, the elevator(s) gravity and a renewable energy source (solar panels in the considered example). Each bond describes the power exchange with the two respective conjugate variables whose product is the power. In this graph, the storage units are represented by the one-port elements, and the energy source are depicted by the two-ports elements to show the energy flows between the system and the exterior. The dynamics of the solar panel and of the mechanical system are modulated by the irridiance and by the mass of passengers respectively.

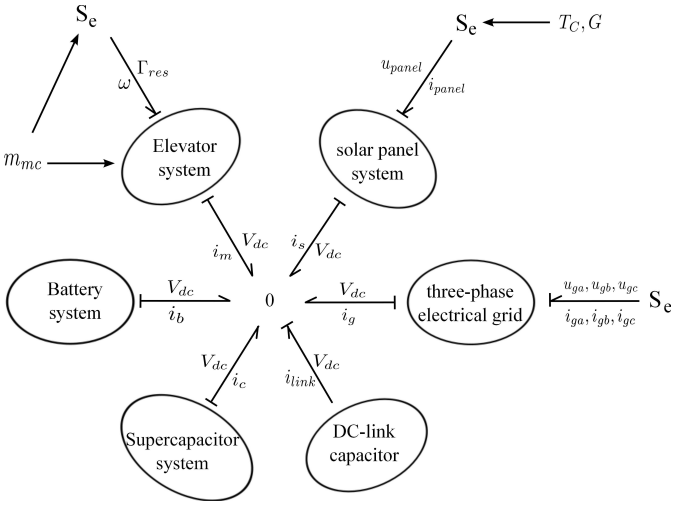

Fig. 2. Microgrid system global structure through a Bond Graph representation.

2.2 Mechanical part, SPMSM and DC/AC converter

In the following, we provide a detailed description of the electro-mechanical subsystem. A first model for the SPMSM and the mechanical dynamics may be found in Yu et al. (2005). The motor dynamic itself, represented in three-phases coordinates, is easy to understand and can be modeled by a Bond Graph as in Rai and Umanand (2008) (but for an asynchronous motor). However in this work, the values of the inductance of the three phases depend on the position of the rotor and besides there is an algebraic constraint on the sum of the three phases voltages. A Park transform may be used to avoid these two problems and describe the motor's dynamic in a reference frame attached to the rotor. It has to be noticed that there is existing result (see Teng et al. (2010)) deriving a Bond Graph model for a synchronous motor but only in the case of smooth poles where the difference between the d and q inductance may be neglected in the mechanical balance equation (see (2)). The Park transform relates the voltages and the currents in two models (the three phases and the two phases models) with "linear" (power conserving) interconnection relations represented by the matrix $\mathcal{P}_1(\theta)$ defined as:

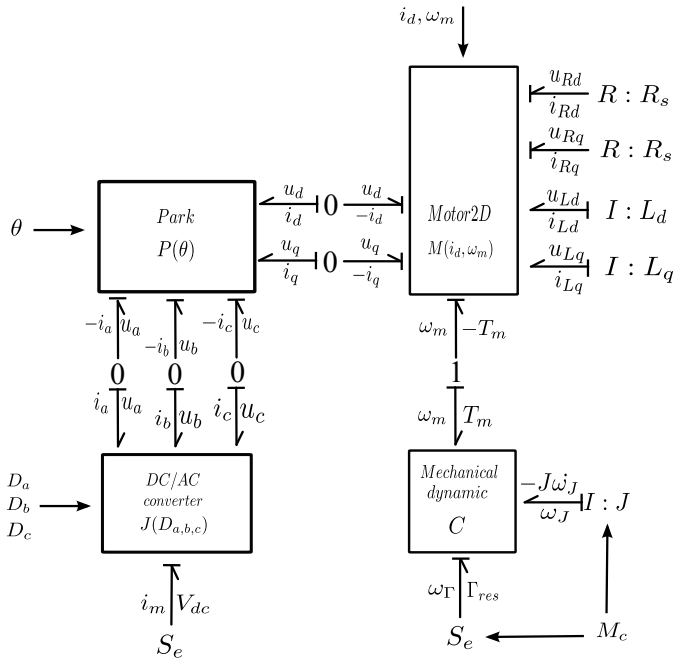

Fig. 3. Bond Graph Model for the electromechanical subsystem

$$\mathcal{P}_1(\theta) = \sqrt{\frac{2}{3}} \begin{bmatrix} cos(p\theta) & cos(p\theta - \frac{2\pi}{3}) & cos(p\theta + \frac{2\pi}{3}) \\ -sin(p\theta) & -sin(p\theta - \frac{2\pi}{3}) & -sin(p\theta + \frac{2\pi}{3}) \end{bmatrix}, \tag{1}$$

where θ is the rotor angle, and p denotes the number of pole pairs. And the converter have been added to define an extension of the corresponding Dirac interconnection structure and control operator (see $\mathcal{J}_m$ and $\mathcal{G}_m$ hereafter), Pham et al. (2014). From that, the explicit structure of the model is described by the Bond Graph in Fig. 3. The state vector is $\mathbf{x}_m = [\, L_d i_d \;\; L_q i_q \;\; J\omega \,]^T$ which represents the magnet fluxes in the stator equivalent phases and the mechanical momentum. The input vector is $\mathbf{u}_m = [\, V_{dc} \;\; \Gamma_{res} \,]^T$ which describes the DC-link voltage and the gravity load torque. The output vector is described by $\mathbf{y}_m = [\, i_m \;\; \omega \,]^T$ which depicts the current from DC-link to system (2) and the angular speed of rotor. Based on these notations, the input-state-output PH form is described as:

$$\begin{cases} \dot{\mathbf{x}}_m = [\mathcal{J}_m(\mathbf{x}_m) - \mathcal{R}_m(\mathbf{x}_m)] \left(\dfrac{\partial H_m(\mathbf{x}_m)}{\partial \mathbf{x}_m} \right)^T + \\ \qquad\qquad + \mathcal{G}_m(\mathbf{x}_m)\mathbf{u}_m, \\ \mathbf{y}_m = \mathcal{G}_m^T(\mathbf{x}_m) \left(\dfrac{\partial H_m(\mathbf{x}_m)}{\partial \mathbf{x}_m} \right)^T, \end{cases} \tag{2}$$

where

$$H_m(\mathbf{x}_m) = \frac{1}{2}\mathbf{x}_m^T \mathcal{M}_m \mathbf{x}_m \text{ with } \mathcal{M}_m = \begin{bmatrix} \frac{1}{L_d} & 0 & 0 \\ 0 & \frac{1}{L_q} & 0 \\ 0 & 0 & \frac{1}{J} \end{bmatrix}, \tag{3}$$

$$\mathcal{J}_m(\mathbf{x}_m) = \begin{bmatrix} 0 & pL_q\omega & 0 \\ -pL_q\omega & 0 & -k(\mathbf{x}_m) \\ 0 & k(\mathbf{x}_m) & 0 \end{bmatrix} \tag{4}$$

$$\text{with } k(\mathbf{x}_m) = \sqrt{1.5}p\psi_f + p(L_d - L_q)i_d, \tag{5}$$

$$\mathcal{R}_m = \begin{bmatrix} R_s & 0 & 0 \\ 0 & R_s & 0 \\ 0 & 0 & 0 \end{bmatrix}, \tag{6}$$

$$\mathcal{G}_m(\mathbf{x}_m) = \begin{bmatrix} \mathcal{P}_1(\theta) & 0 \\ 0 & 1 \end{bmatrix} \begin{bmatrix} k_{ma} & 0 \\ k_{mb} & 0 \\ k_{mc} & 0 \\ 0 & 1 \end{bmatrix}. \tag{7}$$

The control matrix $\mathcal{G}_m(\mathbf{x}_m)$ defined in (7) is derived from the combination of the Park block and the DC/AC converter block in the Fig. 3 which transforms the DC voltage to the motor voltages in the two axis model. Therefore, the control variables (k_{ma}, k_{mb}, k_{mc}) depend on the duty cycles (D_{ma}, D_{mb}, D_{mc}) which are the ratios of transistors on/off times in the converter controlled by a Pulse Width Modulation (PWM) method.

2.3 Energy storage unit

In this section, we provide a PH model for the battery system which is the connection of a lead-acid battery model and DC/DC converter model. An ideal model would consider that the voltage is constant during the charge or discharge periods. It would be useful only in case of low load and current (when compared to the battery's maximal capacity). If it is not the case or for lifetime predictions we need to take into account some nonlinear effects which affects the available charge (see Jongerden and Haverkort (2009)). Electrical circuit models exist (such as in Ceraolo (2000), Durr et al. (2006) or Coupan et al. (2010)) which describe the battery dynamics accurately, but are too complex for an application to the real time optimal power balancing problem. Esperilla, Esperilla et al. (2007) proposed a Bond Graph battery model where the parameters are difficult to identify.

Thus, we need a simple model which can explain the increase/decrease of voltage with charging/discharging current and state of charge, the decrease in capacity with increasing charge or discharge rates, the recovery effect and the hysteresis by using a internal variable, γ_b. There are at least two possible analytical models: the diffusion model, Rakhmatov and Vrudhula (2001) and the Kinetic Battery Model (KiBaM), Manwell and McGowan (1993). Although these models have been developed separately, the KiBaM model can be considered as a first order approximation of the diffusion model, Jongerden and Haverkort (2009). In that sense, the KiBaM is a good choice for our work, Lifshitz and Weiss (2014).

The Bond Graph in Fig. 4 describes the energy flow in the battery unit. The state vector is chosen as $\mathbf{x}_b = [q_b \quad \gamma_b \quad \phi_{Lb}]^T$, representing the internal battery charges and the linkage flux of the DC/DC converter. The input and output vectors are respectively the voltage of DC-link, $\mathbf{u}_b = V_{dc}$, and the current from DC-link to the battery unit, $\mathbf{y}_b = i_b$. The PH model for the battery and the DC/DC converter may be described as:

$$\begin{cases} \dot{\mathbf{x}}_b = [\mathcal{J}_b(\mathbf{x}_b) - \mathcal{R}_b(\mathbf{x}_b)] \left(\dfrac{\partial H_b(\mathbf{x}_b)}{\partial \mathbf{x}_b} \right)^T + \mathcal{G}_b(\mathbf{x}_b)\mathbf{u}_b, \\ \mathbf{y}_b = \mathcal{G}_b^T(\mathbf{x}_b) \left(\dfrac{\partial H_b(\mathbf{x}_b)}{\partial \mathbf{x}_b} \right)^T. \end{cases} \tag{8}$$

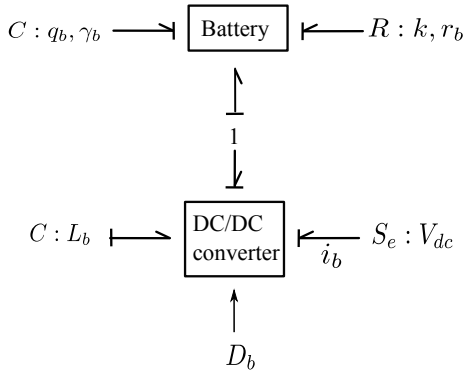

Fig. 4. Bond Graph Model for the battery system

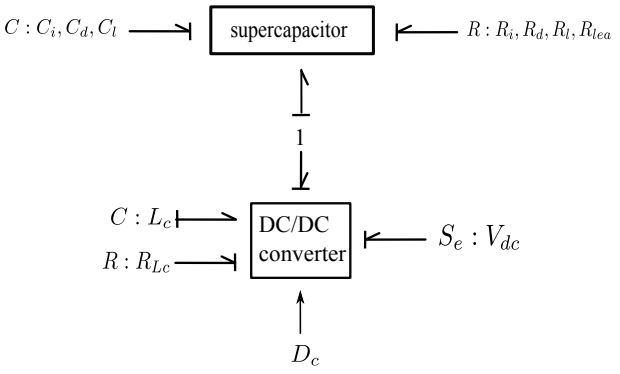

Fig. 5. Bond Graph Model of the supercapacitor system.

where

$$H_b(\mathbf{x}_b) = \frac{1}{2}\mathbf{x}_b^T \mathcal{M}_b \mathbf{x}_b + U_{min} q_b$$
$$\text{with } \mathcal{M}_b = \begin{bmatrix} ac & 0 & 0 \\ 0 & ac^2(1-c) & 0 \\ 0 & 0 & \dfrac{1}{L_b} \end{bmatrix}, \tag{9}$$

which describes the chemical energy stored in the battery and the magnetic energy in the converter inductance,

$$\mathcal{J}_b = \begin{bmatrix} 0 & 0 & -1 \\ 0 & 0 & -\dfrac{1}{c} \\ 1 & \dfrac{1}{c} & 0 \end{bmatrix}, \tag{10}$$

which describes the battery power exchange interconnection,

$$\mathcal{R}_b(\mathbf{x}_b) = \begin{bmatrix} 0 & 0 & 0 \\ 0 & \dfrac{k}{ac^3(1-c)^2} & 0 \\ 0 & 0 & r_b \end{bmatrix}, \tag{11}$$

which represents the battery internal/external dissipation and the converter dissipation, and

$$\mathcal{G}_b = [0 \quad 0 \quad D_b]^T, \tag{12}$$

which depicts the control signal of converter by the duty cycle (D_b) in PWM method.

2.4 Supercapacitor

In this section we develop the PH model for the supercapacitor. Supercapacitors are suitable for power application. They have high performances in energy supplying thanks to a special physical structure based on the electrolytic capacitor, Lai et al. (1992). They usually contain two parallel electrodes with an electrolyte without chemical reaction because of an added separator. The simplest model contains only a RC circuit but it has been shown that it can not fit the experimentally observed non-linear rise and fall of the voltage, in particular after the charging and discharging stops. A more elaborated model is constructed by the parallel connection of three RC branches and of a leakage resistor. It leads to a non-linear responses with three time scales, Zubieta and Bonert (2000). The PH model of the subsystem used hereafter is the connection of the DC/DC converter model and this three-branch supercapacitor model. The state vector of the component (supercapacitor and DC/DC converter) is chosen as $\mathbf{x}_c = [q_{Ci} \quad q_{Cd} \quad q_{Cl} \quad \phi_{Lc}]^T$ which represents the battery internal charges and the magnetic flux of the converter. The input $\mathbf{u}_b = V_{dc}$ describes the DC-link voltage. The output $\mathbf{y}_b = i_c$ depicts the current from DC-link to converter. The Bond Graph of the supercapacitor is shown in Fig. 5. The PH model to describe the system by using these definitions is:

$$\begin{cases} \dot{\mathbf{x}}_c = [\mathcal{J}_c(\mathbf{x}_c) - \mathcal{R}_c(\mathbf{x}_c)] \left(\dfrac{\partial H_c(\mathbf{x}_c)}{\partial \mathbf{x}_c} \right)^T + \mathcal{G}_c(\mathbf{x}_c)\mathbf{u}_c, \\ \mathbf{y}_c = \mathcal{G}_c^T(\mathbf{x}_c) \left(\dfrac{\partial H_c(\mathbf{x}_c)}{\partial \mathbf{x}_c} \right)^T, \end{cases} \tag{13}$$

where

$$H_c(\mathbf{x}_c) = f(q_{Ci}) + \frac{1}{2}\frac{q_{Cd}^2}{C_d} + \frac{1}{2}\frac{q_{Cl}^2}{C_l} + \frac{1}{2}\frac{\phi_{Lc}^2}{L_c}, \tag{14}$$

which describes the energy stored in the supercapacitor and in the converter inductance,

$$\mathcal{J}_c = \begin{bmatrix} 0 & -\mathcal{G}_1/s \\ -\mathcal{G}_1^T/s & 0 \end{bmatrix}, \tag{15}$$

which describes the power interconnection of the supercapacitor unit,

$$\mathcal{R}_c(x_c) = \begin{bmatrix} \mathcal{R}_0 + \mathcal{G}_1\mathcal{G}_1^T/s & 0 \\ 0 & -1/s - R_{Lc} \end{bmatrix}, \tag{16}$$

$$\mathcal{G}_c = [0 \quad 0 \quad 0 \quad -D_c]^T. \tag{17}$$

The values of $\mathcal{G}_1 \in \mathbb{R}^{3\times 1}, \mathcal{G}_0 \in \mathbb{R}^{3\times 3}, s \in \mathbb{R}$ are computed from the supercapacitor resistors. The duty cycle D_c is the control signal of the DC/DC converter in the PWM method and is defined as the ratio of the on/off times for the DC/DC converter "switch" (ideal transistor model).

2.5 DC-link capacitor

The DC-link contains only a capacitor to reduce the DC-link voltage fluctuation. Its PH model is given as:

$$\begin{cases} \dot{\mathbf{x}}_{link} = \mathbf{u}_{link}, \\ \mathbf{y}_{link} = \left(\dfrac{\partial H_{link}(\mathbf{x}_{link})}{\partial \mathbf{x}_{link}} \right)^T, \end{cases} \tag{18}$$

where, $\mathbf{x}_{link} = C_{link}V_{dc}$, $\mathbf{u}_{link} = i_{link}$, $\mathbf{y}_{link} = V_{dc}$, $H_{link}(\mathbf{x}_{link}) = \frac{1}{2}C_{link}V_{dc}^2$.

2.6 Three-phase electrical grid

In our system, we assume that the system of three-phase electrical network is symmetric and does not depend

on the lift system. It is connected to the DC-link by the AC/DC converter. The converter is modeled by the three "switch" pairs that connect the three phases of the external grid, through their three inductors, to the DC-link. The state vector of the subsystem are chosen as $\mathbf{x}_g = [\phi_a \quad \phi_b \quad \phi_c]^T$, the three magnetic fluxes on the inductors. The output of the converter, $\mathbf{u}_g = [u_{ga} \quad u_{gb} \quad u_{gc} \quad V_{dc}]^T$, represents the voltages of the electrical grid and of the DC-link. The output, $\mathbf{y}_g = [i_{ga} \quad i_{gb} \quad i_{gc} \quad i_g]^T$, are the corresponding currents of the mentioned input. The model of the converter is described by the following PH model form:

$$\begin{cases} \dot{\mathbf{x}}_g = \mathcal{G}_g \mathbf{u}_g, \\ \mathbf{y}_g = \mathcal{G}_g^T \left(\dfrac{\partial H_g(\mathbf{x}_g)}{\partial \mathbf{x}_g} \right)^T, \end{cases} \tag{19}$$

where

$$H_g(\mathbf{x}_g) = \frac{1}{2} \frac{\phi_a^2 + \phi_b^2 + \phi_c^2}{L_g}, \tag{20}$$

which describes the magnetic energy stored in the three inductors of three converter phases, $\mathcal{G}_g$ indicates the relation of the three-phase currents and the voltages at the converter ports. This matrix is modulated by the duty cycles (D_{ga}, D_{gb}, D_{gc}) which depend on the on/off times of the converter "switch". The power balance is described as follows:

$$\frac{dH_g}{dt} = u_{ga} i_{ga} + u_{gb} i_{gc} + u_{ga} i_{ga} + V_{dc} i_g. \tag{21}$$

If the phase inductor L_g is small enough, the stored magnetic energy is approximately zero, and the power supplied by the external grid is equal to one supplied to DC-link. The three phases's voltages are considered with a sine form and a phase difference of $2\pi/3$.

2.7 Solar panel

The renewable source investigated in this paper is a power limited solar panel system controlled by the DC/DC converter such as in Kong et al. (2012); Chenni et al. (2007). In practice, the electrical power generated by the panel is less than the absorbed solar power. Furthermore, the ratio "output power/input power" varies nonlinearly with the panel voltage. For the sake of simplicity, we consider that the subsystem (PV and DC/DC converter) model is made of the converter model connected with an energy source whose conjugate variables have a nonlinear constraint mentioned hereafter. Therefore the model is described in the PH form as:

$$\begin{cases} \dot{\mathbf{x}_s} = -R_s \left(\dfrac{\partial H_s(\mathbf{x}_s)}{\partial \mathbf{x}_s} \right)^T + \mathcal{G}_s \mathbf{u}_s, \\ \mathbf{y}_s = \mathcal{G}_s^T \left(\dfrac{\partial H_s(\mathbf{x}_s)}{\partial \mathbf{x}_s} \right)^T, \end{cases} \tag{22}$$

where the state vector $\mathbf{x}_s = \phi_{Ls}$ is the magnetic flux of the converter inductor, $H_s(\mathbf{x}_s) = \frac{1}{2} \frac{\phi_{Ls}^2}{L_s}$ represents the energy stored in the converter inductor, the input $\mathbf{u}_s = [u_{sp} \quad V_{dc}]^T$ represents the voltages on the two ports of the converter corresponding to the DC-link voltage and the panel voltage, the output $\mathbf{y}_s = [i_{sp} \quad i_s]^T$ are the corresponding currents of the inputs, $\mathcal{G}_s = [1 \quad -D_s]$ describes the connection of the energy sources to the state space and D_s is the duty cycle of the DC/DC converter.

3. CONSTRAINTS

3.1 Constraints on the SPMSM and the mechanical system

The constraints of this subsystem are derived from the limits of the three-phase voltages and currents of the machine. These limits are caused by the bounds of the DC-link voltage and of the machine temperature (see Lemmens et al. (2014) for details). On the other hand, because of the machine design and the passenger's comfort requirements, the rotor speed and the rotor acceleration need to be less than a priori chosen values (23). Finally, there are also obvious constraints on the position of the elevator. All these constraints may be summarized as below:

$$\begin{cases} i_d^2 + i_q^2 \leq I_{max}^2, \\ |\omega| \leq \omega_{max}, \\ |\dot{\omega}| \leq a_{max}, \\ \omega(0) = \omega(t_f) = 0, \\ \dot{\omega}(0) = \dot{\omega}(t_f) = 0, \\ \displaystyle\int_0^{t_f} \omega(t) dt = \theta_f, \\ \Gamma_{res} = constant, \\ D_{ma}, D_{mb}, D_{mc} \in \{0, 1\}. \end{cases} \tag{23}$$

3.2 Constraints on the battery system

The energy stored in the battery is used mainly to guarantee the operation of the lift system in emergency situations (where eventually no other power sources are available). However, provided the corresponding minimal level of charge is guaranteed, it may also be used to optimize the total energy cost of the lift systems. Because of the material limit, the battery can not store an infinite amount of energy, Lifshitz and Weiss (2014); Prodan and Zio (2014). Then, the battery charge must be limited in the fixed range (q_{bmin}, q_{bmax}), where $q_{bmax} > q_{bmin} > 0$. Moreover, the rate of charge/ discharge needs to remain between some bounds which are here given as $I_{bmax} > 0$ and $I_{bmin} < 0$. Likewise, the battery voltage must remain in a positive range (U_{bmin}, U_{bmax}). We assume that the converter is able to satisfy these battery constraints. These constraints may then be expressed as:

$$\begin{cases} \begin{bmatrix} q_{bmin} \\ \dfrac{q_{min} - q_b(t)}{1-c} \\ L_b I_{bmin} \end{bmatrix} \leq x \leq \begin{bmatrix} q_{bmax} \\ \dfrac{q_{max} - q_b(t)}{1-c} \\ L_b I_{bmax} \end{bmatrix}, \\ D_b \in \{0, 1\}. \end{cases} \tag{24}$$

3.3 The three-phase electrical grid

On the external grid, the main constraints is the binary values of the control signals that indicates the limited values can be generated from DC-link voltage.

$$D_{ga}, D_{gb}, D_{gc} \in \{0, 1\}. \tag{25}$$

Besides this constraint, another interesting problem useful for the cost minimization is the electrical price profile.

These profiles generally depend on the moment in a day, a month, a year. An optimal scheduling may be derived from electrical price historical data (which may be found for instance in europe energy (2015)) and from the lift moves predictions (and corresponding electrical consumption).

3.4 The solar panel system

On the solar panel system, the constraints are due to the limitations on the irradiance and to the voltage-current characteristic for the considered solar panel. Hence, this section will show the voltage-current curve of the solar source mentioned in the panel model. This curve depends on the panel design (referent temperature and referent irridiance), on the real panel temperature and on the solar irridiance. To find the curve, we will make use of the mathematical approximation of the voltage-current characteristic from Kong et al. (2012); Chenni et al. (2007) because of their good practical results.

$$i_{sp} = I_L(G, T_C) - I_D(i_{sp}, u_{sp}), \tag{26}$$

where

$$I_L(G, T_C) = \frac{G}{G_R}\left[I_{L,R} + \mu_{ISC}\left(T_C - T_{C,R}\right)\right], \tag{27}$$

$$I_D(i_{sp}, u_{sp}) = I_0(T_C)\left[e^{\frac{q(u_{sp}+i_{sp}R_{sp})}{\gamma k T_C}} - 1\right], \tag{28}$$

$$I_0(T_C) = I_{0,R}\left(\frac{T_C}{T_{C,R}}\right)^3 e^{\frac{q\epsilon_G}{kA}\left(\frac{1}{T_{C,R}} - \frac{1}{T_C}\right)}. \tag{29}$$

From this constraint, we can see that the prediction of the solar irridiance is very important for the panel using. These solar power profiles depend on the weather condition (cloud at first) and on the motion cycle of the earth that can be calculated easily. Some reference data are proposed in Heat-Web (2000).

4. OPTIMIZATION OBJECTIVES FOR ENERGY MANAGEMENT

4.1 Objective for the electromechanical conversion subsystem (Mechanical part, SPMSM and DC/AC converter)

The two important objectives we will focus on are the minimization of the dissipated energy in the machine and the tracking of the desired angular velocity profile. We will follow Botan et al. (2010) and use the following criterium for the control of the SPMSM:

$$V_m(D_{ma}, D_{mb}, D_{mc}) = \alpha \int_0^{t_f} \frac{\partial^T H_m(x_m)}{\partial x_m} R_m \frac{\partial H_m(x_m)}{\partial x_m} dt + \beta \int_0^{t_f} (x_{m3} - \overline{\omega})^2 dt \tag{30}$$

with the weights $\alpha, \beta \in R^+$. So, to reach this objective, the d-q voltages is controlled indirectly by regulating the duty cycles (D_{ma}, D_{mb}, D_{mc}) subject to the constraint (23).

4.2 Objective of the solar panel system

This subsystem is a renewable energy source which depends on the weather. We will therefore choose to take the maximal available energy by maximizing the instantaneous absorbed power from the solar panel, hence using the cost function defined as:

$$V_s(u_{sp}) = -u_{sp}(i_{sp})i_{sp}. \tag{31}$$

A popular controller to realize this objective is the Maximum Power Point Tracking (MPPT), Femia et al. (2008),Cabal et al. (2007). By this method, the DC/DC converter duty cycle D_s is regulated to reach the maximum power.

4.3 Global objective and constraints

The energy management of the system can be investigated in two different cases. The first case is when the three-phase electrical is available, the energy consumption cost of the microgrid needs to be minimized. In this case, the global problem we are considering results in the optimal management of the battery and super-capacitor storage levels and in the scheduling of the lift system moves. A potential candidate for the (global) cost function is then:

$$V = \int_{day} P_e(t)[u_{ga}(t)i_{ga}(t) + u_{gb}(t)i_{gb}(t) + u_{gc}(t)i_{gc}(t)]dt. \tag{32}$$

where $P_e(t)$ denotes the price of the electrical power delivered by the external grid.

The second case is in emergency situations where the lift system is autonomous (without the electrical grid connection), the elevator operation need to be guaranteed for a given duration (and number of journeys), without any renewable energy supply Prodan and Zio (2014). This means that the fault events must be detected and that the energy stored in the available storage devices must be sufficient enough for the required autonomous moves of the lift. For this second situation we should thus focus on the fault detection problem, on the maximal operation time without solar panel supply and on the analysis of Mean Time to Failure (MTTF) and Mean Time to Repair (MTTR) for the considered lift system.

5. CONCLUSIONS

This paper introduced a Port Hamiltonian system model for typical lift system microgrid. The model takes into account the nonlinear dynamics of the components controlled by the corresponding converters. It describes the internal power exchanges between all the subsystems explicitly and expresses the network structure of the microgrid (interconnection structure) and the components in a unified PH formalism. Physical limitations and operational requests are formalized as constraints for this state vector representation. Some objectives cost functions for the components and for the global power balancing in the microgrids have been proposed as well. Finally, numerical values of the parameters for the model are listed in tables in the appendix. They have been obtained by direct measurements or identification algorithms. The short term future works in this project concern the development of

a flatness based control of the SPMSM machine (and its connection with Casimir functions of the PH model) and the application of Model based Predictive Control in the case of interconnected PH systems to manage the power balancing problem at the microgrid level.

ACKNOWLEDGEMENT

This work has been partially funded by the Artemis ARROWHEAD project under grant agreement number 332987. All the authors would like to thank warmfully C. Chomel, Q. Crignon and C. Duhoux, from SODIMAS® *ascenseurs*, for their kind cooperation and support.

REFERENCES

Botan, C., Ratoi, M., Ostafi, F., and Horga, V. (2010). Minimum energy control of servo drive systems with pmsm. In *Proceeding of the IEEE International Symposium on Power Electronics, Electrical Drives, Automation and Motion*, 19–23. IEEE, Pisa.

Cabal, C., Alonso, C., Cid-Pastor, A., Estibals, B., Seguier, L., Leyva, R., Schweitz, G., and Alzieu, J. (2007). Adaptive digital mppt control for photovoltaic applications. In *Proceeding of the IEEE International Symposium on Industrial Electronics ISIE 2007*, 2414–2419. IEEE, Vigo, Spain.

Ceraolo, M. (2000). New dynamical model of lead-acid batteries. *IEEE Transactions on Power Systems*, 15(4), 1184–1190.

Chenni, R., Makhlouf, M., Kerbache, T., and Bouzid, A. (2007). A detailed modeling method for photovoltaic cells. *Energy*, 32(9), 1724–1730.

Coupan, F., Sadli, I., Marie-Joseph, I., Primerose, A., and Clergeot, H. (2010). New battery dynamic model: Application to lead-acid battery. In *Proceeding of the IEEE International Conference on Computer and Automation Engineering*, volume 5, 140–145. IEEE, Singapore.

Durr, M., Cruden, A., Gair, S., and McDonald, J. (2006). Dynamic model of a lead acid battery for use in a domestic fuel cell system. *Journal of Power Sources*, 161(2), 1400–1411.

Esperilla, J., Félez, J., Romero, G., and Carretero, A. (2007). A model for simulating a lead-acid battery using bond graphs. *Simulation Modelling Practice and Theory*, 15(1), 82–97.

europe energy (2015). Europe's energy. URL `https://www.energy.eu/`.

Femia, K., Lisi, G., Petrone, G., Spagnuolo, G., and Vitelli, M. (2008). Distributed maximum power point tracking of photovoltaic arrays: Novel approach and system analysis. *IEEE Transactions on Industrial Electronics*, 55(7), 2610–2621.

Heat-Web (2000). Netgreen heat website. URL `http://www.promote.netgreendevelopments.com`.

Jongerden, M. and Haverkort, B. (2009). Which battery model is use? *Software, Institution of Engineering and Technology*, 3(6), 445–457.

Kong, K., Mamat, M., Ibrahim, M., and Muzathik, A. (2012). New approach on mathematical modeling of photovoltaic solar panel. *Applied Mathematical Sciences*, 6(8), 381–401.

Lagorse, J., Paire, D., and Miraoui, A. (2010). A multi-agent system for energy management of distributed power sources. *Renewable Energy*, 35(1), 174–182.

Lai, J., Levy, S., and Rose, M. (1992). High energy density double-layer capacitors for energy storage applications. In *Aerospace and Electronic Systems Magazine*, volume 7, 14–19. IEEE.

Lemmens, J., Vanassche, P., and Driesen, J. (2014). Pmsm drive current and voltage limiting as a constraint optimal control problem. *accepted for the IEEE Journal of Emerging and Selected Topics in Power Electronics*, pp(99), 1.

Lifshitz, D. and Weiss, G. (2014). Optimal energy management for grid-connected storage systems. *accepted for the Optimal Control Application and Methods*.

Manwell, J. and McGowan, J. (1993). Lead acid battery storage model for hybrid energy systems. *Solar Energy*, 50(5), 399–405.

Mohammedi, M., Becherif, M., Ayad, M., Kraa, O., Aboubou, A., and Bahri, M. (2013). Passivity based control and fuzzy logic estimation applied to dc hybrid power source using fuel cell and supercapacitor. In *Proceedings of the 3rd International Conference on Systems and Control*, 77–82. IEEE, Algiers, Algeria.

Nuno, E., Ortega, R., Jayawardhana, B., and Basanez, L. (2013). Coordination of multi-agent euler lagrange systems via energy shaping: Networking improves robustness. *Automatica*, 49(10), 3065–3071.

Paire, D., Simoes, M., Lagorse, J., and Miraoui, A. (2010). A real-time sharing reference voltage for hybrid generation power system. In *IEEE Industry Applications Society Annual Meeting*, 1–8. IEEE, Houston, TX.

Parisio, A., Rikos, E., and Glielmo, L. (2014). A model predictive control approach to microgrid operation optimization. *IEEE Transactions on Control Systems Technology*, 22(5), 1813–1827.

Pham, T., L.Lefevre, Genon-Catalot, D., and Pham, V. (2014). An energy-based control model for autonomous lifts. In *Proceeding of the 40th IEEE Annual Conference on Industrial Electrical Society*, 4286–4292. IEEE, Dallas, TX, USA.

Prodan, I. and Zio, E. (2014). A model predictive control framework for reliable microgrid energy management. *Electrical Power and Energy Systems*, 61, 399–409.

Rai, B.U. and Umanand, L. (2008). Bond graph model of doubly fed three phase induction motor using the axis rotator element for frame transformation. In *Simulation Modelling Practice and Theory*, volume l6, 1704–1712.

Rakhmatov, D. and Vrudhula, S. (2001). An analytical high-level battery model for use in energy management of portable electronic systems. In *Proceedings of the IEEE/ACM International Conference on Computer-Aided Design*, 488–493. IEEE, San Jose, CA, USA.

Schiffer, J., Ortega, R., Astolfi, A., Raisch, J., and Sezi, T. (2014). Stability of synchronized motions of inverter based microgrids under droop control. In *Proceeding of the 19th IFAC World Congress*, 6361–6367. IFAC, Cape Town, South Africa.

Teng, L., Yanjie, L., and Lining, S. (2010). Bond graph model of permanent magnet linear synchronous motor. In *Proceeding of the 2nd IEEE International Conference on Industrial and Information Systems*, volume 2, 128–131. IEEE, Dalian.

Table 1. Loads of the microgrid system

Parameter	Description	Value
	AC/DC converter, SPMSM, mechanical part	
$m_{mc}[kg]$	mass of cabin	200
$m_{mw}[kg]$	the mass of counterweight	400
$r_m[m]$	radial of pulley	0.026
$g[m/s^2]$	gravity acceleration	9.81
$L_d[H]$	direct inductance of the machine stator	
$L_q[H]$	quadrature inductance of the machine stator	
p	number of pole pairs	6
$R_s[\Omega]$	phase resistance of stator	
$J[kg.m^2]$	inertia of the mechanical part	0.4
$\Gamma_{res}[N.m]$	load torque generated by the effect of the gravity on the elevator	50.8
$i_d, i_q[A]$	stator currents	
$\omega[rad/s]$	rotor speed	
$\overline{\omega}[rad/s]$	rotor speed reference	
$i_m[A]$	current from DC-link to the DC/AC converter	
$\mathcal{P}_1(\theta) \in R^{2\times 3}$	Park matrix, Pham et al. (2014)	
$\theta[rad]$	rotor angle	
$k_{ma}, k_{mb}, k_{mc} \in R$	control parameters of converter	
$I_{max}[A]$	limit of the current magnitude	
$U_{max}[V]$	limit of the voltage magnitude	
$\omega_{max}[rad/s]$	limit of the speed	
$a_{max}[rad/s^2]$	limit of the acceleration	
$t_f[s]$	displacement duration	
$\theta_f[rad]$	rotor angle after a displacement	
$\mathbf{x}_m \in \mathbb{R}^3$	state vector	
$\mathbf{u}_m, \mathbf{y}_m \in \mathbb{R}$	input and output	
$\mathcal{J}_m, \mathcal{R}_m \in \mathbb{R}^{3\times 3}$	interconnection and dissipation matrices	
$\mathcal{G}_m \in \mathbb{R}^{3\times 1}$	input matrix	
$H_m \in \mathbb{R}$	Hamiltonian	
$D_{ma}, D_{mb}, D_{mc} \in \{0,1\}$	converter state	
V_m	cost function of the machine optimization	

Yang, N., Paire, D., Gao, F., and Miraoui, A. (2014). Distributed control of dc microgrid considering dynamic responses of multiple generation units. In *Proceedings of the 40th IEEE Annual Conference of Industrial Electronics Society*, 2063–2068. IEEE, Dallas, TX, USA.

Yu, H., Wang, H., and Zhao, K. (2005). Energy-shaping control of pm synchronous motor based on hamiltonian system theory. In *Proceedings of the IEEE Eighth International Conference on Electrical Machines and Systems*, volume 2, 1549–1553. IEEE, Nanjing.

Zubieta, L. and Bonert, R. (2000). Characterization of double-layer capacitors for power electronics applications. *IEEE Transaction on Industry Applications*, 36(1), 199–205.

6. TABLES OF PARAMETERS

Table 2. Energy storage units of the microgrid

Parameter	Description	Value
	Battery system, Manwell and McGowan (1993)	
$a[F^{-1}]$	voltage parameters	0.04
$c \in (0,1)$	internal charge ratio	0.4
$k[s^{-1}]$	internal resistor	0.58
$L_b[H]$	inductance of DC/DC converter	0.0025
$r_b[\Omega]$	resistance of the battery system	0.015
$U_{min}[V]$	minimum allowed internal discharge	48
$q_b[A.s]$	battery charge	
$\gamma_b[A.s]$	internal disposition charge	
$\phi_{Lb}[V.s]$	inductance flux linkage of DC/DC converter	
$i_b[A]$	current from DC-link to converter	
U_{bmin}, $U_{bmax}[V]$	minimum and maximum voltage limits of battery	
I_{bmin}, $I_{bmax}[A]$	minimum and maximum current limits of battery	
q_{bmin}, $q_{bmax}[C]$	minimum and maximum charge limits of battery	
$\mathbf{x}_b \in \mathbb{R}^3$	state vector	
$\mathbf{u}_b, \mathbf{y}_b \in \mathbb{R}$	input and output	
$\mathcal{J}_b, \mathcal{R}_b \in \mathbb{R}^{3\times 3}$	interconnection and dissipation matrices	
$\mathcal{G}_b \in \mathbb{R}^{3\times 1}$	input matrix	
$H_b \in \mathbb{R}$	Hamiltonian	
$D_b \in \{0,1\}$	converter state	
	Super-capacitor system	
$C_{i0}[F]$	immediate branch internal capacitor	11.074
$C_{i1}[F/V]$	immediate branch internal voltage-dependent capacitor	0.05
$C_d[F]$	delay branch internal capacitor	0.315
$C_l[F]$	low branch internal capacitor	0
$L_c[H]$	converter inductance	0.00025
$R_{Lc}[\Omega]$	converter resistor	0.144
$R_i[\Omega]$	immediate branch internal resistance	0
$R_d[\Omega]$	delay branch internal resistance	147.8
$R_l[\Omega]$	low branch internal resistance	inf
$R_{lea}[\Omega]$	leakage resistance	inf
q_{Ci}, q_{Cd}, $q_{Cl}[C]$	three-branch charges	
$\phi_{Lc}[V.s]$	inductance flux linkage of DC/DC converter	
$i_c[A]$	current from DC-link to converter	
$\mathbf{x}_c \in \mathbb{R}^4$	state vector	
$\mathbf{u}_c, \mathbf{y}_c \in \mathbb{R}$	input and output	
$\mathcal{J}_c, \mathcal{R}_c \in \mathbb{R}^{4\times 4}$	interconnection and dissipation matrices	
$\mathcal{G}_c \in \mathbb{R}^{4\times 1}$	input matrix	
$H_c(\mathbf{x}_c) \in \mathbb{R}$	Hamiltonian	
$D_c \in \{0,1\}$	converter state	
	DC link	
$C_{link}[F]$	DC-link capacitor	0.039
$V_{dc}[V]$	DC-link voltage	100
I_{cmin}, $I_{cmax}[A]$	minimum and maximum current limits of super-capacitor	
U_{cmin}, $U_{cmax}[V]$	minimum and maximum voltage limits of super-capacitor	
$i_{link}[A]$	current from DC-link to capacitor	
$\mathbf{x}_{link} \in \mathbb{R}$	state vector	
$\mathbf{u}_{link}, \mathbf{y}_{link} \in \mathbb{R}$	input and output	
$H_{link} \in \mathbb{R}$	Hamiltonian	

Table 3. Energy generation units of the micro-grid system

Parameter	Description	Value
	Three-phase electrical grid	
$L_g[H]$	phase inductance of the grid connection	0.002
$U_{grid}[V]$	voltage amplitude of three-phase electrical grid	
$f_{grid}[V]$	frequency of three-phase electrical grid	
$P_e(t)[€/Wh]$	electrical price	
ϕ_a, ϕ_b, $\phi_c[V.s]$	flux linkages of the three phases of the electrical grid connection	
$u_a, u_b, u_c[V]$	three-phase grid voltages	
$i_a, i_b, i_c[A]$	three-phase grid currents	
$i_g[A]$	current from DC-link to converter	
$k_{ga}, k_{gb}, k_{gc} \in R$	control parameters of converter	
$\mathbf{x}_g \in \mathbb{R}^3$	state vector	
$\mathbf{u}_g, \mathbf{y}_g \in \mathbb{R}^4$	input and output	
$\mathcal{J}_g, \mathcal{R}_g \in \mathbb{R}^{3\times3}$	interconnection and dissipation matrices	
$\mathcal{G}_g \in \mathbb{R}^{3\times4}$	input matrix	
$H_g \in \mathbb{R}$	Hamiltonian	
$D_{ga}, D_{gb}, D_{gc} \in \{0,1\}$	converter state	
	Solar panel system, Kong et al. (2012)	
$R_s[\Omega]$	converter resistance	0.035
$L_s[H]$	converter inductance	0.001
$R_{sp}[\Omega]$	series resistance	1.713
$u_{sp}[V]$	panel voltage	
$i_{sp}[A]$	panel current	
$\phi_{Ls}[H]$	converter inductance flux linkage	
$i_s[A]$	current from converter to DC-link	
$I_{L,R}[A]$	light current at reference condition	
$I_0[A]$	reverse saturation actual current	
$I_{0,R}[A]$	reverse saturation current at the reference condition	
$T_C[K]$	cell actual temperature	298
$T_{C,R}[K]$	cell temperature at the reference condition	
$G[W/m^2]$	actual irridiance	1000
$G_R[W/m^2]$	irridiance at the reference condition	
$q[C]$	electron charge	$1.6.10^{-19}$
$\gamma = A.NCS.NS$	shape factor	15.4
$k[J/K]$	Boltzmann constant	$1.4.10^{-23}$
A	completion factor	0.7
NCS	number of cells connected in series per module	11
NS	number of modules connected in series of the entire array	2
$\mu_{ISC}[A/K]$	manufacturer supplied temperature coefficient of short-circuit current	0.1
$\epsilon_G[eV]$	material band gap energy (1.12 eV for Si, 1.35 eV for GaGs)	1.5
$\mathbf{x}_s \in \mathbb{R}$	state vector	
$\mathbf{u}_s, \mathbf{y}_s \in \mathbb{R}^2$	input and output	
$\mathcal{J}_s, \mathcal{R}_s \in \mathbb{R}$	interconnection and dissipation matrices	
$\mathcal{G}_s \in \mathbb{R}^{1\times2}$	input matrix	
$H_s \in \mathbb{R}$	Hamiltonian	
$D_s \in \{0,1\}$	converter state	
V_s	solar panel cost function	